

Enhanced pool boiling critical heat flux induced by capillary wicking effect of a Cr-sputtered superhydrophilic surfaces

Hong Hyun Son, Gwang Hyeok Seo, Sung Joong Kim*
Department of Nuclear Engineering, Hanyang University
222 Wangsimri-ro, Seongdong-gu, Seoul 04763, Republic of Korea
hhsn@hanyang.ac.kr, seokh@hanyang.ac.kr,
*Corresponding author: sungkim@hanyang.ac.kr

1. Introduction

The film growth mechanism by physical vapor deposition (PVD) sputtering shows an intrinsic tendency to keep the surface smooth by eliminating microstructures [1]. In light of boiling heat transfer, the smooth surface potentially reduces active nucleation of bubbles and rewetting of dry spots near the critical heat flux (CHF). This kind of process is highly likely to deteriorate the CHF. Thus, it is essential to produce appropriate microstructures on the surface for the enhancement of the CHF. In this study, to investigate the microstructural effect of thin film-fabricated surfaces on the pool boiling CHF, we controlled the surface roughness in a narrow range of 0.1-0.25 μm and its morphologies, in the form of micro-scratches using PVD sputtering technique. Specifically for DC magnetron sputtering, pure chromium (Cr) was selected as a target material owing to its high oxidation resistance.

In order to analyze the CHF trend with changes in roughness, we introduced existing capillary wicking-based models because superhydrophilic characteristics of microstructures are highly related to the capillary wicking behaviors in micro-flow channels. Using the capillary wicking-based model, a force balance, resulting in capillary-induced momentum was slightly modified to be applicable for polished metal surfaces. The surface characteristics were compared using the roughness parameters (i.e., the average roughness R_a and the roughness peak distance R_{sm}) and the spreading behaviors of a liquid droplet.

2. Formation of Cr-based micro/nanostructures and their impact on dynamic wetting performance

In order to simulate different surface roughnesses of Cr-sputtered surfaces, test surfaces were polished with different grits of sandpaper before Cr sputtering. High grits of sandpaper of the microscale were selected with grit numbers of 800, 600, 400, and 320. After polishing, the lower grit number increased the surface roughness gradually, spanning the range from 0.12 to 0.27 μm . In order to carry out successive sputtering processes, contaminants on the polished surfaces were carefully removed using an ethanol solution.

The growth mechanism of the thin film depends on the sputtering parameters, such as substrate temperature, inert gas pressure, exposure time, and DC power [1]. Since the present study focuses on investigating the

roughness effect of Cr-sputtered surfaces on pool boiling CHF, we fixed these parameters to the sputtering conditions, which are summarized in Table I.

Table I: DC sputtering conditions

Sputtering parameter	Target condition
Target material	99.95 % pure Cr
Substrate material	Stainless steel grade 316
Substrate temperature ($^{\circ}\text{C}$)	150 ± 0.3
Exposure time (hour)	1
Working pressure (Torr)	1×10^{-2}
DC power (W)	150 – 160

During an hour of sputtering, an approximately 1 μm Cr thin film was formed with fine columnar grains (Fig. 1(b)). In addition, through energy dispersive spectrum (EDS) mapping analysis (Fig. 1(a)), it was confirmed that the Cr composition in the thin film reaches approximately 96 wt.% with a small quantity of oxygen atoms (~ 3 wt.%). These results indicate that the 1 μm thin film mostly consists of Cr-based structures.

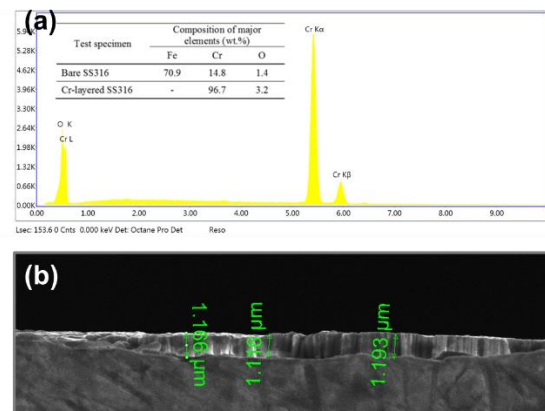


Fig. 1. Composition of major elements (Fe, Cr, and O) on the surfaces using EDAX mapping technique: (a) a phase spectrum of a Cr-sputtered surface and measured compositions of bare and Cr-sputtered surfaces; (b) a fracture cross-section of a Cr layer.

The major roughness parameters measured are the average roughness R_a , the roughness peak distance R_{sm} , and the surface area ratio r . Here, R_a is defined as the arithmetic average height from peaks to valleys in

absolute value, and thus it represents the height variations of the surface. R_{sm} indicates the arithmetic mean value of the width of the roughness, which characterizes the width variations in the surface. r is the surface area ratio of the geometric area to the projected area, typically called the roughness factor. By measuring these parameters at three different points on the surface, the averaged values were obtained as shown in Table II.

Table II: Summary of surface roughness data measured by AFM.

Test specimen	R_a (nm)	R_{sm} (μm)	r (-)
Cr-SP800	101 \pm 4	1.88 \pm 0.09	1.09 \pm 0.02
Cr-SP600	183 \pm 40	2.46 \pm 0.43	1.17 \pm 0.05
Cr-SP400	213 \pm 42	2.86 \pm 0.36	1.15 \pm 0.02
Cr-SP320	258 \pm 45	3.18 \pm 0.50	1.20 \pm 0.002

Figure 2 shows the change of surface morphology before and after Cr sputtering. The polishing process was intended to simulate micro-scratches with a repeated pattern because recent CHF studies [2, 3] have revealed that the major factor that enhances CHF on micro/nanostructured surfaces comes from abundant wicking channels in microscale. If the surface structure varies only in the nanoscale, without micro-cavities, it hardly forms effective wicking channels and active nucleation sites.

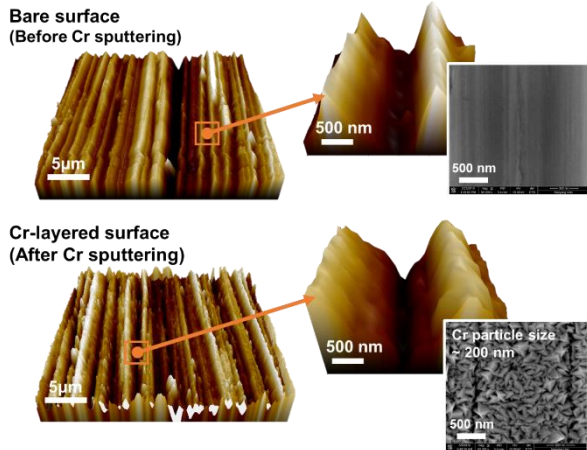


Fig. 2. Change of surface morphologies before and after Cr sputtering.

Cr particles deposited on micro-scratched surfaces changed the hydrophilic wettability of the base surface to superhydrophilic. In order to characterize the dynamic wetting performance of Cr-sputtered surfaces, experiments were conducted to track the spreading history of a liquid droplet. Figure 3(a) shows how the drop base diameter advances over the surface on the millisecond timescale. Under room temperature condition, the advancing drop base diameter was measured by capturing the spreading of a 1 μl liquid droplet with a recording rate at 63 frames/sec. A 1 μl

liquid droplet was fully absorbed within 800 msec for all surfaces. Thus, we focused on the initial spreading behavior, setting the 0 msec start time as the instant when a distinct drop edge is identifiable to 200 msec, which is the duration sufficient for defining a linearly advancing drop base diameter.

The increasing trend of the averaged advancing rate of drop base diameter is shown in Fig. 3(b). Based on ample evidence of dynamic wetting performance on wicking-dominant surfaces [2-4], these liquid spreading behaviors strongly indicate that the micro-scratched surfaces give abundant wicking channels to enhance capillary-induced flow over the surface.

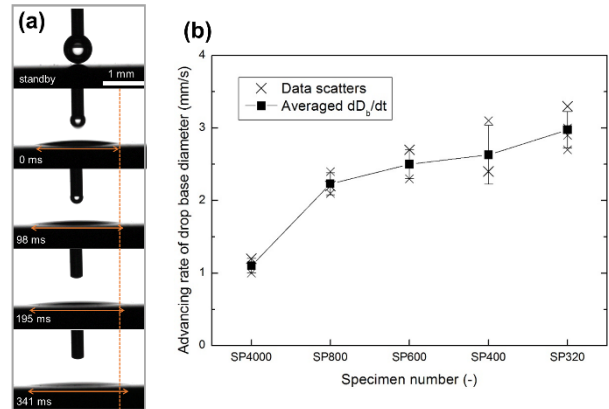


Fig. 3. (a) Dynamic wetting behavior of a 1 μl liquid droplet on Cr-sputtered surfaces. (b) Comparison of averaged advance rate of drop base diameter on a Cr-sputtered surface.

3. Experimental description

As shown in Fig. 4, the test specimen was heated using a DC power supply via copper electrodes connected to each end side of the test specimen.

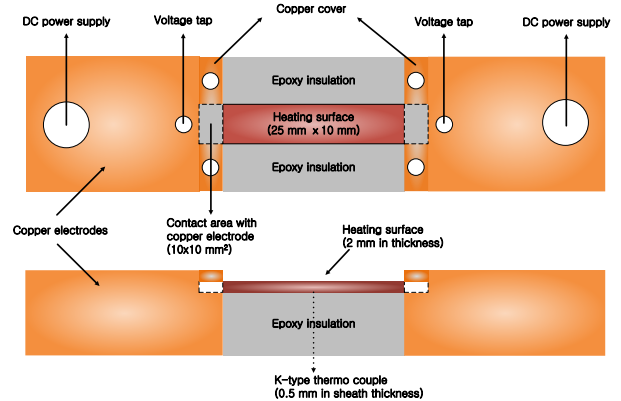


Fig. 4. Schematic of test section.

In order to measure the inner surface temperature opposite to the heat transfer surface and voltage drop along the test specimen, a K-type thermocouple and a pair of voltage taps were attached to the end side of the test specimen. The length, width, and thickness of test specimen are 25, 10, and 2 mm, respectively. The CHF was determined when inner wall temperature jumped

rapidly more than 200 °C or voltage drop also increased due to fast oxidation.

Applied heat flux was calculated using a simple heat flux equation as shown in Eq. (1).

$$q'' = \frac{\text{Power}}{A_{\text{heated}}} = \frac{VI}{WL} \quad (1)$$

V is voltage drop across the length of the heater, I is current, W is width of heater, and L is length of the heater. Using a propagation of error method, measurement uncertainty was estimated as 5.2%.

4. Result and discussion

Pool boiling CHF of all Cr-sputtered surfaces was observed to improve during repetitive tests. In addition, the increasing CHF trend with increasing surface roughness was observed from 32 to 79%. This result indicates that the roughness-augmented superhydrophilic property effectively delays the occurrence of the CHF. Recent CHF studies [2, 3] have reported that successive CHF enhancement on roughness-augmented hydrophilic (or superhydrophilic) surfaces is achieved by capillary wicking, which enhances liquid suction into the dry area beneath growing bubbles.

Figure 5 shows the CHF comparison between present data and the three models related to CHF prediction. Interestingly, these models [3, 5, 6] poorly agree with the observed CHF trend by under-predicting the large enhancements in CHF_{SP400} and CHF_{SP320} for low roughness values. For that reason, when polishing surfaces using different grits of sandpaper, higher average roughness R_a and higher peak distance R_{sm} do not always induces a higher surface area ratio because even a rougher surface sometimes forms a lower roughness peak density. It indicates that r factor cannot be a representative value for present polished metal surfaces.

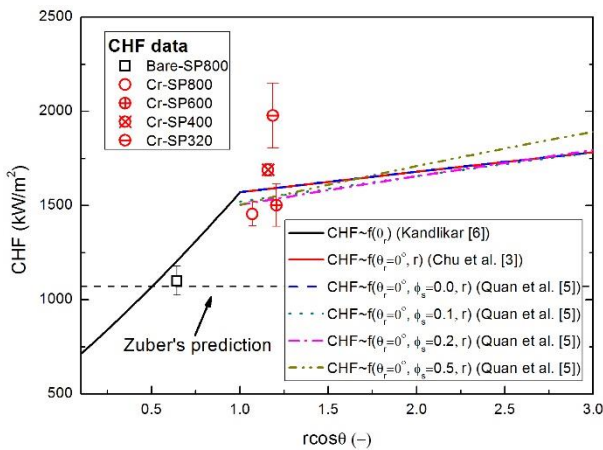


Fig. 5. Comparison of CHF data with the existing correlations based on roughness factor and contact angle.

Recent studies [2] have argued that the capillary wicking effect on Cr-sputtered superhydrophilic surfaces needs to be evaluated in terms of capillary flow dynamics inside wicking-channels rather than using the

conventional approach based on the static force balance of a single bubble.

In order to establish an expression of micro-flow dynamics accessible from measurements of a polished metal surface, it is necessary to simulate artificial capillary flow channels along roughness profiles. Accordingly, it was assumed that micro-flow channels shown in the AFM image can be parameterized as V-shaped capillary flow channels. Then, the morphology of nanostructures by the deposition of Cr particles was neglected for simplification. On polished surfaces, the roughness of peaks and valleys tend to appear in repeated patterns, and thus statistically give standardized roughness parameters obtained by arithmetic calculations. This makes it possible to introduce R_a and R_{sm} values as representative values in defining geometric parameters of a modeled capillary flow channel such as the cross-sectional area A_c , the wetted perimeter p_{wetted} , and the hydraulic diameter D_h . Here, assuming that the height of triangle area is $4R_a$ and the width is R_{sm} , the cross-sectional flow area A_c and the wetted perimeter

p_{wetted} becomes $2R_aR_{sm}$ and $2\sqrt{(4R_a)^2 + 1/4R_{sm}^2}$, respectively. In addition, considering that the hydraulic diameter D_h of the V-shaped area corresponds to the ratio of the cross-sectional flow area A_c to the wetted perimeter p_{wetted} , D_h can be expressed as following Eq. (2).

$$D_h = \frac{A_c}{p_{\text{wetted}}} = \frac{R_a}{\sqrt{16\left(\frac{R_a}{R_{sm}}\right)^2 + 1}} \quad \text{Eq. (2)}$$

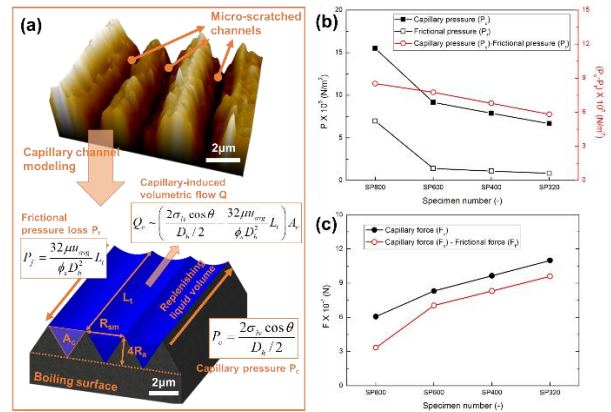


Fig. 6. (a) Schematic of the physical relation between capillary and frictional forces in a modeled capillary flow channel on polished metal surfaces; (b) Pressure balance; (c) Force balance.

Starting from the capillary liquid inflow rate model [4], the effective force F_e activating capillary-driven momentum depends on the force difference between capillary and frictional forces. This governing relation can be expressed as the multiplication of acting pressures and the cross-sectional flow area A_c :

$$F_e = F_c - F_f = (P_c - P_f) A_c \quad \text{Eq. (3)}$$

Here, P_c and P_f are the capillary and frictional pressures, respectively. Inside a modeled capillary flow channel, the capillary pressure follows the Young-Laplace equation, $2\sigma_{lv}\cos\theta/(D_h/2)$. Next, in order to simulate frictional pressure loss P_f along a modeled capillary flow channel, Kim et al. [4] introduced Darcy's law, which defines the pressure drop, $32\mu u_{avg}L_t/(\phi_s D_h^2)$, in laminar flow inside a porous medium. Here, L_t is the travel length of the liquid, which was assumed to be 100 μm in all surfaces.

In consequence, a mathematical form of the effective force was constructed as follows.

$$F_e = P_e A_c = \left(\frac{2\sigma_{lv}\cos\theta}{D_h/2} - \frac{32\mu u_{avg}L_t}{\phi_s D_h^2} \right) A_c \quad \text{Eq. (4)}$$

Here, it was assumed that the liquid inflow velocity u_{avg} is proportional to the advancing rate of liquid droplet diameter dD_b/dt .

The effective force balanced between capillary and frictional forces plays an additional role in enhancing the capillary wicking effect on the CHF. In terms of triggering the CHF, the formation of irreversible dry patches resulting from the rapid evaporation beneath coalesced bubbles, is affected by how much evaporative liquid mass flows into the microlayer. Thus, when the amount of liquid supplied from the surrounding liquid source of dry patches is insufficient for removing the evaporative heat flux, dryout occurs with the propagation of rapid evaporation from the center of dry patches. This indicates that the occurrence of the CHF physically corresponds to the extent of volumetric liquid flow Q_c inside the microlayer around dry patches. Since we have assumed that the liquid inflow velocity u_{avg} is proportional to the advancing rate of liquid droplet diameter dD_b/dt , the volumetric liquid flow Q_c can be derived from the multiplication of the advancing rate of liquid droplet diameter dD_b/dt and the cross-sectional area A_c . Figure 7 shows that the trend of volumetric liquid flow with the effective force is in good agreement with the increasing CHF trend, although roughness factor-based models poorly predicted this increasing CHF trend.

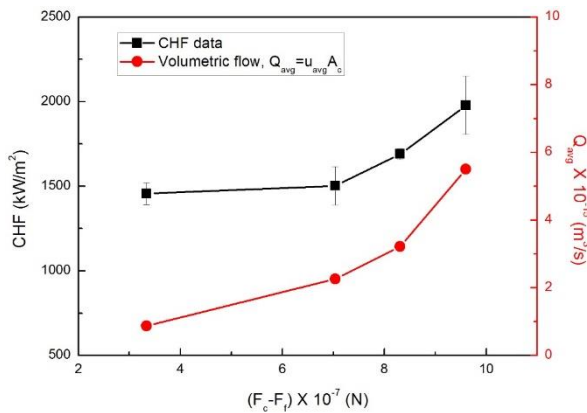


Fig. 7. Comparable relationship between the CHF and the capillary-induced volumetric flow along with the effective force.

5. Conclusions

In this study, we deposited a Cr layer, with an $\sim 1 \mu\text{m}$ thickness, on test surfaces using a DC magnetron sputtering technique. After Cr sputtering under given conditions, the Cr-sputtered surfaces showed superhydrophilic characteristics and its capability became more enhanced with an increase of surface roughness. Judging from spreading behavior of a liquid droplet, the presence of micro-wicking channels, coupled with Cr nanostructures, effectively enhanced the advancing rate of drop base diameter.

The CHF exhibited an increasing trend with increasing surface roughness. However, the enhancement ratio agreed poorly with the predictions of the roughness factor-based models, all of which originated from a conventional static force balance. In contrast, given the assumptions based on capillary flow dynamics, the force balance between the capillary and the frictional forces robustly represented the trend of capillary-induced volumetric flow along with the CHF data.

ACKNOWLEDGEMENT

This research was supported by the Basic Science Research Program through the National Research Foundation of Korea (NRF) funded by the Ministry of Science, ICT & Future Planning (No. 2015R1C1A1A01054861) and the National Research Foundation of Korea (NRF) grant funded by the Korean government (MSIP:Ministry of Science, ICT and Future Planning) (No. 2016R1A5A1013919).

REFERENCES

- [1] M. Nie, N. Kaiser and K. Ellmer, Growth and morphology evolution of semiconducting oxides and sulfides prepared by magnetron sputtering, in: Electrical Engineering and computer science, Technical University of Berlin, 2014.
- [2] N.S. Dhillon, J. Buongiorno and K.K. Varanasi, Critical heat flux maxima during boiling crisis on textured surfaces, Nat Commun, No. 6, 2015.
- [3] K.-H. Chu, R. Enright and E.N. Wang, Structured surfaces for enhanced pool boiling heat transfer, Applied Physics Letters, No. 100, p. 241603, 2012.
- [4] S.H. Kim, G.C. Lee, J.Y. Kang, K. Moriyama, M.H. Kim and H.S. Park, Boiling heat transfer and critical heat flux evaluation of the pool boiling on micro structured surface, International Journal of Heat and Mass Transfer, No. 91, pp. 1140-1147, 2015.
- [5] X. Quan, L. Dong and P. Cheng, A CHF model for saturated pool boiling on a heated surface with micro/nano-scale structures, International Journal of Heat and Mass Transfer, No. 76, pp. 452-458, 2014.
- [6] S.G. Kandlikar, A theoretical model to predict pool boiling CHF incorporating effects of contact angle and orientation, Journal of Heat Transfer, No. 123, pp. 1071-1079, 2001.